High-pressure torsion of iron with various purity levels and validation of Hall-Petch strengthening mechanism

Robert Tejedor, Kaveh Edalati, Jose Antonio Benito, Zenji Horita, Jose Maria Cabrera

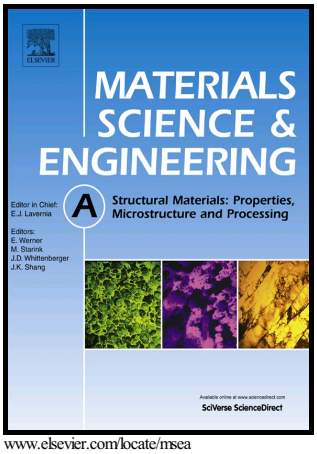

www.elsevier.com/locate/msea

PII: S0921-5093(18)31653-8
DOI: https://doi.org/10.1016/j.msea.2018.11.127
Reference: MSA37247

To appear in: *Materials Science & Engineering A*

Received date: 23 October 2018
Revised date: 24 November 2018
Accepted date: 27 November 2018

Cite this article as: Robert Tejedor, Kaveh Edalati, Jose Antonio Benito, Zenji Horita and Jose Maria Cabrera, High-pressure torsion of iron with various purity levels and validation of Hall-Petch strengthening mechanism, *Materials Science & Engineering A,* https://doi.org/10.1016/j.msea.2018.11.127

High-pressure torsion of iron with various purity levels and validation of Hall-Petch strengthening mechanism

Robert Tejedor[1], Kaveh Edalati[2,3,*], Jose Antonio Benito[1], Zenji Horita[2,3], Jose Maria Cabrera[1]

[1]Universitat Politècnica de Catalunya, Departamento de Ciencia de los Materiales e Ingeniería Metalúrgica, EEBE, Barcelona 08019, Spain
[2]WPI, International Institute for Carbon-Neutral Energy Research (WPI-I2CNER), Kyushu University, Fukuoka 819-0395, Japan
[3]Department of Materials Science and Engineering, Faculty of Engineering, Kyushu University, Fukuoka 819-0395, Japan

[*]Corresponding author: Tel: 0081-92-802-2992; kaveh.edalati@kyudai.jp

Abstract:
Impurity atoms have a significant effect on the strength of metals processed by severe plastic deformation (SPD), but their strengthening mechanism is still under argument. To gain an insight into the strengthening mechanism, iron samples with different purity levels such as 99.96% (IF steel), 99.94% (Armco steel), 99.88% and 97.78% and with different initial states (bulk, powder and ball-milled) were processed by high-pressure torsion (HPT). The steady-state hardness and tensile strength for the materials with the micrometer and submicrometer grain sizes reasonably followed the Hall-Petch relationships reported earlier for pure iron and mild steels. However, the nanograined materials followed an inverse Hall-Petch relationship. It was shown that the occurrence of softening by the inverse Hall-Petch effect can be significantly avoided by stabilizing the grain boundaries using carbon atoms. These findings indicate that the extra hardening by impurity atoms is mainly due to the grain-boundary strengthening mechanism.

Keywords: severe plastic deformation (SPD); ball milling; powder consolidation, ultrafine-grained (UFG) materials; nanostructured metals; reverse Hall-Petch relationship

1. Introduction

Processing metals through the severe plastic deformation (SPD) methods [1,2] such as high-pressure torsion (HPT) [3,4], accumulative roll-bonding (ARB) [5,6], equal channel angular pressing (ECAP) [7,8] and twist extrusion (TE) [9,10] leads to significant grain refinement and resultant high strength and high hardness. Such a hardening is usually attributed to the Hall-Petch effect [11,12], but some studies strongly suggested that the dislocations have a more significant effect than the grain boundaries on the strength of SPD-processed materials [13,14].

Iron (Fe) is among the most investigated metals in the SPD studies. Although there are several attempts to process Fe by ARB [6,15,16], ECAP [17-21] and TE [22], the HPT method has been the most popular processing route for this relatively hard metal [23-67]. The first attempt on HPT processing of Fe appeared in 1935, when Bridgman processed different kinds of metals using the first HPT facility [68]. In 1955, Bridgman processed Fe by HPT again to find an evidence for the ω-phase formation, but his attempt was not successful [69]. More details concerning the old publications on HPT processing of Fe was reviewed in Ref. [70]. The application of HPT to Fe in recent decades started with a work by Valiev *et al.* in 1990, which reported new magnetic properties for ultrafine-grained (UFG) Fe [23]. Following this publication, the focus of majority of works on SPD processing of Fe has been on the microstructural evolutions and enhanced mechanical properties [23-67], although the magnetic properties [56] and phase transformations [31] of UFG Fe are still of interest.

Close examination of publications on HPT processing of Fe indicates that the deviations of reported mechanical properties and grain sizes are in a wide range mainly because of the difference in the purity levels and partly because of the processing routes [15-69]. For example, the reported hardness values for HPT-processed Fe are in a wide range from 300 HV [34] to 1200 HV [60] with the grain sizes ranging from 20 nm [60] to 600 nm [35]. Currently, there is no general agreement on the mechanism of extra hardening by impurity atoms. It was suggested that the impurity atoms can enhance the solution hardening effects in UFG materials by pining the dislocations [71] or they can stabilize the grain boundaries by pining the boundary migration [3,72]. Despite earlier publications on various UFG materials and particularly on Fe, systematic studies are still required to get an insight into the mechanism of extra strengthening by impurity atoms.

In this study, Fe with various purity levels is processed by HPT and the evolutions of hardness, tensile properties and microstructure are investigated. It is shown that the Hall-Petch mechanism [73,74] is reasonably explains the mechanical properties, but a break in the Hall-Petch relationship occurs (i.e. inverse Hall-Petch effect appears [75-77]), when the grain sizes are at the nanometer level. It is also shown that the softening for nanograined Fe can be significantly avoided by stabilizing the grain boundaries using carbon atoms, as attempted by Borchers *et al.* [60].

2. Experimental Materials and Procedures

Four Fe samples with different initial states, different purity levels and different initial grain sizes were received in this study as given in Table 1: discs of IF steel (10 mm diameter and 0.8 mm thickness) with 99.96% purity and 140 μm grain size; discs of Armco steel (10 mm diameter and 0.8 mm thickness) with 99.94% purity and 33 μm grain size, commercially pure Fe powders with 99.88% purity and 10 μm grain size; and ball-milled Fe powders with 97.78% purity and 26 nm grain size (17 hours milling with a speed of 160 rpm and a ball-to-powder mass ratio of 27 under argon atmosphere in stainless steel vial). The chemical compositions in Table 1

were measured by spark analysis for metallic elements, by combustion technique for C and S, and by inert gas fusion technique for O. The grain size of the ball-milled powder was measured by X-ray diffraction using CuKα radiation by employing a modified Williamson-Hall method [78] (contrast factors for every reflection were taken from the works of Revesz *et al.* [79]). The grain sizes of three other materials were measured by optical microscopy after etching using a solution of 90% C_2H_5OH and 5 vol.% HNO_3 for 2 min. Initial microstructures of IF and Armco steels are shown in the optical micrographs of Figs. 1(a) and (b), respectively, and the appearance of commercially pure and ball-milled Fe powders are shown in the scanning electron microscopy (SEM) images of Figs. 1(c) and (d), respectively.

As given in Table 2, the HPT process was carried out at room temperature (300 K) or at 473 K using a facility having a pair of anvils made of tool steel. There was a shallow hole with 10 mm diameter and 0.25 mm depth at the center of each anvil. Each disc sample or 0.6 g of powders was placed on the hole of lower anvil. After compression under a pressure of P = 2 GPa or 6 GPa, the samples were strained by rotating the lower anvil with respect to the upper anvil for N = 1/8 to 20 turns with a rotation speed of 0.2 rpm or 1.0 rpm. Since Fe (99.96%) is rather soft and an earlier study showed that its steady-state hardness is the same after processing under 2 and 6 GPa [37], the material was processed under a pressure of 2 GPa to reduce the damages to the HPT anvils.

After HPT processing, the samples with the processing conditions given in Table 2 were examined by Vickers microhardness, tensile test and transmission electron microscopy (TEM), described below.

First, the disc samples were polished to mirror-like surfaces and their Vickers microhardness was measured using a load of 200 g for Fe (99.96%) and 500 g for Fe (99.94%), Fe (99.88%) and Fe (99.78%) with 15 s duration. The hardness of all HPT-processed discs were measured at 8 different radial directions with 0.5 mm increments. The average values of hardness at each distance from the disc center was evaluated as a function of equivalent von-Mises strain, as attempted in Ref. [34]. The hardness of ball-milled powder was evaluated by Vickers indentations with a load of 100 g after mounting and polishing.

Second, the disc samples were polished on both sides and their thickness was reduced to 0.5-0.6 mm. Thereafter, miniature tensile specimens having 0.6-1 mm gauge width and 1-1.5 mm gauge length were cut from the samples using an electric discharge wire-cutting machine and were pulled to failure with an initial strain rate of 3.3×10^{-3} s^{-1}. See Refs. [34,80] for the detailed geometry of tensile specimens.

Third, small discs with 3 mm in diameter were cut from 2-5 mm away from the center of discs processed by HPT for N = 20 and their thickness was reduced to 0.1 mm by smooth mechanical grinding. The 3 mm discs were further thinned for electron transparency with a twin-jet electrochemical polisher using a solution of 90 vol.% CH_3COOH and 10 vol.% $HClO_4$ with an applied voltage of 14 V at ambient temperature. The microstructures of samples were examined by TEM at 200 or 300 kV using bright-field images, dark-field images and selected area electron diffraction (SAED) patterns. The average grain sizes were estimated from the dark-field images by measuring the two orthogonal axes of the bright areas for more than 50 grains.

3. Results

Figure 2 shows the variation of hardness against the distance from disc center for Fe samples with the purity levels of (a) 99.96%, (b) 99.94%, (c) 99.88 % and (d) 97.78% after HPT processing for 1/8-20 turns. For the samples with the purity levels of 99.96%, 99.94% and

99.88 %, the hardness increases with increasing the distance from the disc center and with increasing the number of turns, and the hardness values are higher than the initial hardness levels. The hardening with increasing the distance from the disc center and number of turns is simply due to the strain hardening effect. Figure 2(c) shows that the hardening rate is smaller, when the processing temperature is higher. However, the maximum hardness levels are relatively similar after processing at room temperature and 473 K. For the samples with a purity level of 97.78%, the hardness values are reasonably independent of the number of turns and of the distance from the disc center and all hardness data are below the hardness levels for the initial nanograined ball-milled powders. Such a strain-induced softening by HPT processing was reported earlier when the initial materials have unstable nonograined structure such as in electrodeposited Ni [4,81], cryomilled Cu [82] and electrodeposited Ni-Fe [83].

The influence of strain on hardening and softening behaviors of four selected alloys are shown more clearly in Fig. 3, where all hardness values in Fig. 2 are plotted as a function of von-Mises equivalent strain ($\varepsilon=\gamma/\sqrt{3}$ in which $\gamma=2\pi rN/h$; γ: shear strain; r: distance from disc center, N: number of turns, h: average disc thickness [2,34]). Examination of Fig. 3 indicates several main points.

(i) All hardness data for each material fall well on a single curve, indicating that the strain is the main factor determining the hardness levels.

(ii) For the samples with the purity levels of 99.96%, 99.94% and 99.88%, the hardness increases with increasing the strain and finally saturates to the steady states. The hardness values for the samples processed for 20 turns fall well at the steady states and are reasonably independent of strain. The occurrence of steady state at large strains is due to a balance between the formation and annihilation of lattice defect such as dislocations and grain boundaries [4]. This behavior at large strains was reported in a wide range of metals [84-88] and alloys [3,54] with moderate or high melting temperatures.

(iii) For the samples with a purity level of 97.78%, the hardness level after HPT decrease below a level for the initial state. This softening behavior was reported when the initial material has unstable noanograins [81-83], when the material transforms to the phases that are softer than the initial phase [89,90], when the metals with low melting temperatures such as In, Sn, Pd and Zn are processed by HPT [91,92], or when ultrahigh pure metals with moderate melting temperature such as Al are processed at ambient or cryogenic temperature [93,94]. The former case should be the reason for the softening of ball-milled Fe (97.78%) powders in this study.

(iv) For the Fe (99.88%) powders, the rate of hardening is slower after HPT processing at 473 K when compared with that after processing at ambient temperature. This is a natural consequence of low strain hardening rates at higher temperatures [4].

(v) The steady-state hardness levels significantly increase with increasing the purity level from 306 Hv for Fe (99.94%) to 610 Hv for Fe (97.78%). The mechanism for this extra hardening by impurity atoms will be discussed in the discussion session.

Tensile stress-strain curves are shown in Fig. 4 for the HPT-processed Fe samples with the purity levels of (a) 99.96%, (b) 99.94%, (c) 99.88 % and (d) 97.78%. The general trend is that the strength increases after HPT processing, but the ductility decreases. Moreover, the increase in the strength is more significant, when the number of HPT turns increases due to the strain hardening effect. For the Fe (99.88%) powder, the high strength and slight ductility suggest the occurrence of good consolidation, especially when the samples are processed at elevated temperature. The current results together with numerous publications on consolidation

of various kinds of crystalline and amorphous powders and chips [95-99] confirm the potential of HPT for cold or low-temperature consolidation. For the ball-milled Fe (97.78%) powder, despite processing at 473 K, all samples break in the elastic region, indicating that their consolidation is not perfect. Further heat treatment of this sample at 848-923 K resulted in improving the ductility and decreasing the strength, as discussed in the Appendix and shown in Fig. A1.

TEM bright-field images, dark-field images and corresponding SAED patterns are shown in Fig. 5 for the Fe samples with the purity levels of (a) 99.96%, (b) 99.94%, (c, d) 99.88 % and (e) 97.78% after HPT processing for 20 turns, where (a-c) were processed at room temperature and (d, e) were processed at 473 K. For all samples, the SAED pattern exhibits a complete ring form, indicating that the microstructures consist of small grains with random misorientations. It is also evident from both bright-field and dark-field images that the grain sizes are at the submicrometer or even nanometer level. Statistic measurement of the grain sizes using the dark-field images suggests that the average steady-state grain sizes for Fe (99.96%), Fe (99.94%) and Fe (99.88%) processed at room temperatures are 350±120 nm, 340±50 nm and 230±70 nm, respectively. The average grain size for Fe (99.88%) and Fe (97.78%) processed at 473 K are 240±50 nm and 110±70 nm. The unusual grain growth of ball-milled powder after HPT processing is consistent with the grain coarsening reported earlier in a few other HPT-processed nanograined metallic materials [81-83] and oxides [100,101]. The measured grain sizes are consistent with the strength and hardness of different Fe samples after HPT processing at room temperature and 473 K. Taken all together, these results confirm that the grain size of Fe decreases with increasing the impurity level, in good agreement with the earlier reports on HPT-processing of other meals [4,54,92].

4. Discussion

Extra strengthening by increasing the amount of impurity atoms can be described by three possible scenarios. First, the extra strengthening by impurity atoms is due to enhanced solid solution hardening, as suggested by Rupert *et al.* for nanograined materials [71]. However, an earlier publication confirmed that the effect of solution hardening on the total hardness is less than 15% for a wide range of HPT-processed metallic materials [54]. Second, impurity atoms can pin the motion of dislocations and increase the density of dislocations [102,103], as there are strong supports concerning the significance of dislocations on the hardening of HPT-processed materials [13,104]. The X-ray peak profile analysis is currently the main method that is used to evaluate the density of dislocations [105], but the estimated values by this indirect method are usually much higher than those measured directly by TEM observations, as shown in a few publications on Cu [106], Fe [107] and Cu [108]. Therefore, in the authors' view, precise examination of the effect of dislocations is quite difficult because of the current drawbacks in the estimation of real dislocation density. Third, the solute atoms pin the grain boundary mobility and reduce the grain size, which is consistent with the experimental data presented in this manuscript. The significant effect of grain size on the hardness of UFG materials was shown earlier for various kinds of metals [44] and alloys [54]. As discussed below, one reasonable approach to examine the extra strengthening by impurity atoms is to compare the data achieved in this study for HPT-processed Fe with the Hall-Petch relationships reported earlier for Fe.

Numerous studies reported equations for the Hall-Petch strengthening mechanism in pure Fe (see a review in [109]), and among them the equation reported by the group of Takaki is one of the most reliable one, which was verified by comprehensive studies [110-112].

$$\sigma\,[\mathrm{MPa}] = 100 + 600\,d\,[\mu\mathrm{m}]^{-1/2} \quad (1)$$

In this equation, σ is the strength and d is the average grain size. Another equation, that could reasonably explain the strength versus grain size relation in low-purity Fe and mild steels, was proposed by William and Hashemi [113].

$$\sigma\,[\mathrm{MPa}] = 70 + 0.74\,d\,[\mathrm{m}]^{-1/2} \quad (2)$$

A compression between these two equations and the data achieved in this study is shown in Fig. 6. It should be noted that the hardness values in Fig. 6 were converted to normal strength by dividing the hardness by a factor of 3 [114]. Figure 6 shows several important points.

First, the data for both tensile strength and hardness reasonably follow the Hall-Petch relationships suggested by Takaki *et al.* [110-112] and William and Hashemi [113]. This indicates that the reduction of grain size and grain boundary strengthening are mainly responsible for the extra hardening by impurity atoms. It should be noted that the data reported by Benito *et al.* for Fe with various carbon levels after ball milling and hot consolidation [115] also follow the Hall-Petch relationship, as discussed in the Appendix and shown in Fig. A2. The deviations of the data in Figs. 6 and A2 should be mainly due to effect of carbon on the slope of Hall-Petch plot, as discussed by Takaki [112]. Another reason for the deviations is the contribution of other strengthening mechanisms.

Second, the ball-milled Fe (97.78%) with an average grain size of 26 nm exhibits an apparent break in the Hall-Petch relationship. Note that the grain size for the ball-milled powder was measured by X-ray line profile analysis, but the size should be reliable because the method gives very good consistency with the TEM measurements when the grain sizes are below 30 nm (see a review by Ungar in [116]). Moreover, since the hardness for ball-milled powders were measured directly on the powders by a mounting technique, the hardness levels deviate significantly. However, as shown in Fig. 6, the hardness of this sample is below the Hall-Petch level even by considering the standard deviations. The softening effect in the ball-milled powder, which was reported as an inverse or reverse Hall-Petch effect in different nanometals [75-77], is due to the contribution of grain-boundary-mediated processes through the dislocation-based mechanism, diffusion-based mechanism, grain-boundary-shearing mechanism and two-phase-based mechanism, as discussed by Carlton and Ferreira [117]. It should be noted that molecular dynamic simulation predicted a break in the Hall-Petch relationship for Fe at grain sizes smaller than 14.7 nm [118]. Moreover, experimental studies suggested that the inverse Hall-Petch effect is enhanced in Fe in the presence of solute atoms [119].

Third, Borchers *et al.* attempted to stabilize the grain boundaries of nanograined Fe by carbon atoms through co-milling of Fe and 0.4 wt.% C followed by HPT processing [60]. Figure 6 shows that the hardness of their materials, having 20-23 nm, is so close to the reported Hall-Petch relationship, indicating that the inverse Hall-Petch relationship can be significantly avoided by stabilizing the grain boundaries using the impurity atoms. Similar approach was recently employed by Hu *et al.* to avoid the inverse Hall-Petch effect in electrodeposited Ni-Mo [72]. Taken all together, the current data suggests that the Hall-Petch strengthening mechanism is the dominant mechanism determining the effect of impurity atoms on the hardening of UFG Fe.

Finally, it should be noted that Starink recently proposed a model regarding the strengthening mechanisms of severely deformed materials [14]. He concluded that the classic Hall-Petch relationship includes both grain-boundary strengthening mechanism and the

dislocation strengthening mechanism because of the correlations between these two mechanisms. Dieter also suggested similar idea decades ago regarding the correlation between the dislocation density and grain size [120]. Despite the ideas presented in these publications, separating the magnitude of dislocation strengthening and grain-boundary strengthening in the Hall-Petch relationship remains as an open question due to current limitations in the estimation of real dislocation density.

5. Conclusions

Iron with different purities (99.96%, 99.94%, 99.88% and 97.78%) and different initial states (bulk, powder and ball-milled) was severely deformed by high-pressure torsion (HPT) and the following conclusions were drawn

(1) The hardness and tensile strength increased and the steady-state grain size decreased with the reduction of purity level regardless of the initial state and processing route.

(2) The mechanical properties could be reasonably explained by the Hall-Petch relationships reported for pure iron and mild steels, but an inverse Hall-Petch relationship was observed by decreasing the grain size to the nanometer level.

(3) It was concluded that the strengthening by impurity atoms is mainly due to the Hall-Petch grain boundary strengthening mechanism.

Appendix

Figure A1 shows the tensile stress-strain curves for the ball-milled Fe (97.78%) powders after HPT processing for 20 turns at 473 K and post-HPT annealing at 848-923 K for 1 h. While the sample annealed at 848 K breaks in the elastic region without showing any ductility, the samples annealed at higher temperatures exhibit improvement in the ductility. Increasing the annealing temperature improves the tensile ductility, but reduces the strength. The current results suggest that although all HPT-processed samples (regardless of their purity level or grain size) exhibit poor ductility at the steady state, the combination of strength and ductility can be improved by selecting appropriate post-HPT annealing conditions.

Figure A2 shows a compression between the mechanical properties achieved by Benito *et al.* for Fe with various carbon contents after ball milling followed by hot consolidation at different temperatures [115] with the Hall-Petch plots reported by Takaki *et al.* [110-112] and by William and Hashemi [113]. Despite some scatterings especially for the samples with high carbon contents, the data points can be reasonably described by the Hall-Petch plots, indicating the significance of grain boundaries on strengthening. As discussed by Takaki [111], the slope of Hall-Petch plot increases with increasing the carbon content and this should be the main reason for the scattering of data points in Fig. A2. Another reason for the scattering should be due to effect of other strengthening factors such as dislocations and solute atoms.

Acknowledgements

This study was supported by Grants-in-Aid for Scientific Research from the MEXT, Japan (16H04539, 26220909). The HPT process was carried out at IRC-GSAM, Kyushu University, Japan.

References

[1] R.Z. Valiev, R.K. Islamgaliev, I.V. Alexandrov, Bulk nanostructured materials from severe plastic deformation, Prog. Mater. Sci. 45 (2000) 103-189.

[2] R.Z. Valiev, Y. Estrin, Z. Horita, T.G. Langdon, M.J. Zehetbauer, Y.T. Zhu, Producing bulk ultrafine-grained materials by severe plastic deformation, JOM 58(4) (2006) 33-39.
[3] A.P. Zhilyaev, T.G. Langdon, Using high-pressure torsion for metal processing: fundamentals and applications, Prog. Mater. Sci. 53 (2008) 893-979.
[4] R. Pippan, S. Scheriau, A. Taylor, M. Hafok, A. Hohenwarter, A. Bachmaier, Saturation of fragmentation during severe plastic deformation, Annu. Rev. Mater. Res. 40 (2010) 319-343.
[5] P. Metenier, G. Gonzales-Doncel, O.A. Ruano, J. Wolfenstine, O.D. Sherby, Superplastic behavior of a fine-grained two-phase Mg-9wt.%Li alloy, Mater. Sci. Eng. A 125 (1990) 195-202.
[6] Y. Saito, H. Utsunomiya, N. Tsuji, T. Sakai, Novel ultra-high straining process for bulk materials: Development of the accumulative roll-bonding (ARB) process, Acta Mater. 47 (1999) 579-583.
[7] V.M. Segal, V.I. Reznikov, A.E. Drobyshevskiy, V.I. Kopylov, Plastic working of metals by simple shear, Russian Metall. 1 (1981) 99-105.
[8] R.Z. Valiev, T.G. Langdon, Principles of equal-channel angular pressing as a processing tool for grain refinement, Prog. Mater. Sci. 51 (2006) 881-981.
[9] Y. Beygelzimer, V. Varukhin, S. Synkov, A. Sapronov, V. Synkov. New techniques for accumulating large plastic deformations using hydroextrusion, Fizika i Tekhnika Vusokih Davlenii 9 (1999) 499-508.
[10] Y. Beygelzimer, V. Varyukhin, S. Synkov, D. Orlov, Useful properties of twist extrusion, Mater. Sci. Eng. A 503 (2009) 14-17.
[11] Y.T. Zhu, T.G. Langdon, Influence of grain size on deformation mechanisms: an extension to nanocrystalline materials, Mater. Sci. Eng. A 409 (2005) 234-242.
[12] A. Azushima, R. Kopp, A. Korhonen, D.Y. Yang, F. Micari, G.D. Lahoti, P. Groche, J. Yanagimoto, N. Tsuji, A. Rosochowski, A. Yanagida, Severe plastic deformation (SPD) processes for metals, CRIP Ann. Mauuf. Techn. 57 (2008) 716-735.
[13] M.J. Starink, X.C. Cheng, S. Yang, Hardening of pure metals by high-pressure torsion: a physically based model employing volume-averaged defect evolutions, Acta Mater. 61 (2013) 183-192.
[14] M.J. Starink, Dislocation versus grain boundary strengthening in SPD processed metals: non-causal relation between grain size and strength of deformed polycrystals, Mater. Sci. Eng. A 705 (2017) 42-45.
[15] N. Tsuji, Y. Ito, Y. Saito, Y. Minamino, Strength and ductility of ultrafine grained aluminum and iron produced by ARB and annealing, Scripta Mater. 47 (2002) 893-899.
[16] E. Bonnot, A.L. Helbert, F. Brisset, T. Baudin, Microstructure and texture evolution during the ultra grain refinement of the Armco iron deformed by accumulative roll bonding (ARB), Mater. Sci. Eng. A 561 (2013) 60-66.
[17] B.Q. Han, F.A. Mohamed, E.J. Lavernia, Mechanical properties of iron processed by severe plastic deformation, Metall. Mater. Trans. A 34 (2003) 71-83.
[18] M. Sus-Ryszkowska, T. Wejrzanowski, Z. Pakieła, K.J. Kurzydłowski, Microstructure of ECAP severely deformed iron and its mechanical properties, Mater. Sci. Eng. A 369 (2004) 151-156.
[19] B.Q. Han, E.J. Lavernia, F.A. Mohamed, Dislocation structure and deformation in iron processed by equal-channel-angular pressing, Metall. Mater. Trans. A 35 (2004) 1343-1350.

[20] A.V. Panin, A.A. Panina, Y.F. Ivanov, Deformation macrolocalisation and fracture in ultrafine-grained armco iron, Mater. Sci. Eng. A 486 (2008) 267-272.
[21] H.S. Kim, W.S. Ryu, M. Janeck, S.C. Baik, Y. Estrin, Effect of equal channel angular pressing on microstructure and mechanical properties of IF steel, Adv. Eng. Mater. 7 (2005) 43-46.
[22] E. Pashinska, V. Varyukhin, S. Dobatkin, A. Zavdoveev, Mechanisms of structure formation in low-carbon steel at warm twist extrusion, Emerg. Mater. Res. 2 (2013) 138-143.
[23] R.Z. Valiev, R.R. Mulyukov, V.V. Ovchinnikov, Direction of grain-boundary phase in submicrometre-grained iron, Philos. Mag. Lett. 62 (1990) 253-256.
[24] Y.V. Ivanisenko, A.V. Korznikov, I.M.Safarov, R.Z. Valiev, Formation of submicrocrystalline structure in iron and its alloys after severe plastic deformation, Nanostruct. Mater. 6 (1995) 433-436.
[25] R.Z. Valiev, Y.V. Ivanisenko, E.F. Rauch, B. Baudelet, Structure and deformation behaviour of Armco iron subjected to severe plastic deformation, Acta Mater. 44 (1996) 4705-4712.
[26] F. Wetscher, A. Vorhauer, R. Pippan, Strain hardening during high pressure torsion deformation, Mater. Sci. Eng. A 410-411 (2005) 213-216.
[27] M.V. Degtyarev, L.M. Voronova, T.I. Chashchukhina, Grain growth upon annealing of armco iron with various ultrafine-grained structures produced by high-pressure torsion deformation, Phys. Met. Metallogr. 99 (2005) 276-285.
[28] Y. Ivanisenko, R.Z. Valiev, H.J. Fecht, Grain boundary statistics in nanostructured iron produced by high pressure torsion, Mater. Sci. Eng. A 390 (2005) 159-165.
[29] M. Sus-Ryszkowska, Z. Pakieła, R.Z. Valiev, J.W. Wyrzykowski, K.J. Kurzydłowski, Mechanical properties of nanostructured iron obtained by various methods of severe plastic deformation, Solid State Phenomen. 101-102 (2005) 85-90.
[30] F. Wetscher, R. Pippan, Cyclic high-pressure torsion of nickel and Armco iron, Philos. Mag. 86 (2006) 5867-5883.
[31] Y. Ma, E. Selvi, V.I. Levitas, J. Hashemi, Effect of shear strain on the α–ε phase transition of iron: a new approach in the rotational diamond anvil cell, J. Phys.: Condens. Matter 18 (2006) S1075-S1082.
[32] M.V. Degtyarev, T.I. Chashchukhina, L.M. Voronova, A.M. Patselov, V.P. Pilyugin, Influence of the relaxation processes on the structure formation in pure metals and alloys under high-pressure torsion, Acta Mater. 55 (2007) 6039-6050.
[33] A. Vorhauer, R. Pippan, On the onset of a steady state in body-centered cubic iron during severe plastic deformation at low homologous temperatures, Metall. Mater. Trans. A 39 (2008) 417-429.
[34] K. Edalati, T. Fujioka, Z. Horita, Evolution of mechanical properties and microstructures with equivalent strain in pure Fe processed by high pressure torsion, Mater. Trans. 50 (2009) 44-50.
[35] Y. Todaka, Y. Miki, M. Umemoto, C. Wang, K. Tsuchiya, Tensile property of submicrocrystalline pure Fe produced by HPT-straining, Mater. Sci. Forum 584−586 (2008) 597−604.

[36] K. Edalati, Z. Horita, T.G. Langdon, The significance of slippage in processing by high-pressure torsion, Scripta Mater. 60 (2009) 9-12.
[37] K. Edalati, Z. Horita, Universal plot for hardness variation in pure metals processed by high-pressure torsion, Mater. Trans. 51 (2010) 1051-1054.
[38] A. Hohenwarter, C. Kammerhofer, R. Pippan, The ductile to brittle transition of ultrafine-grained Armco iron: an experimental study, J. Mater. Sci. 45 (2010) 4805-4812.
[39] B. Oberdorfer, B. Lorenzoni, K. Unger, W. Sprengel, M. Zehetbauer, R. Pippan, R. Wurschum, Absolute concentration of free volume-type defects in ultrafine-grained Fe prepared by high-pressure torsion, Scripta Mater. 63 (2010) 452-455.
[40] A. Hohenwarter, R. Pippan, Anisotropic fracture behavior of ultrafine-grained iron, Mater. Sci. Eng. A 527 (2010) 2649-2656.
[41] Y. Mine, Z. Horita, Y. Murakami, Effect of high-pressure torsion on hydrogen trapping in Fe–0.01 mass% C and type 310S austenitic stainless steel, Acta Mater. 58 (2010) 649-657.
[42] J.A. Benito, R. Tejedor, R. Rodríguez-Baracaldo, J.M. Cabrera, J.M. Prado, Ductility of bulk nanocrystalline and ultrafine grain iron and steel, Mater. Sci. Forum 633-634 (2010) 197-203.
[43] K. Edalati, R. Miresmaeili, Z. Horita, H. Kanayama, R. Pippan, Significance of temperature increase in processing by high-pressure torsion, Mater. Sci. Eng. A 528 (2011) 7301-7305.
[44] K. Edalati, Z. Horita, High-pressure torsion of pure metals: Influence of atomic bond parameters and stacking fault energy on grain size and correlation with hardness, Acta Mater. 59 (2011) 6831-6836.
[45] K. Edalati, Z. Horita, Correlation of physical parameters with steady-state hardness of pure metals processed by high-pressure torsion, Mater. Sci. Forum 667-669 (2011) 683-688.
[46] S. Descartes, C. Desrayaud, E.F. Rauch, Inhomogeneous microstructural evolution of pure iron during high-pressure torsion, Mater. Sci. Eng. A 528 (2011) 3666-3675.
[47] K. Edalati, Z. Horita, Correlations between hardness and atomic bond parameters of pure metals and semi-metals after processing by high-pressure torsion, Scripta Mater. 64 (2011) 161-164.
[48] K. Edalati, Z. Horita, Parameters influencing steady-state grain size of pure metals processed by high-pressure torsion, Mater. Sci. Forum 706-709 (2012) 3034-3039.
[49] K. Edalati, Z. Horita, Continuous high-pressure torsion, J. Mater. Sci. 45 (2010) 4578-4582.
[50] K. Edalati, S. Lee, Z. Horita, Continuous high-pressure torsion using wires, J. Mater. Sci. 47 (2012) 473-473.
[51] V.P. Pilyugin, L.M. Voronova, M.V. Degtyarev, T.I. Chashchukhina, Structure refinement of pure iron during low-temperature high-pressure deformation, Russ. Metall. 2012 (2012) 297-302.
[52] J. Ning, E. Courtois-Manara, L. Kurmanaeva, A.V. Ganeev, R.Z. Valiev, C. Kubel, Y. Ivanisenko, Tensile properties and work hardening behaviors of ultrafine grained carbon steel and pure iron processed by warm high pressure torsion, Mater. Sci. Eng. A 581 (2013) 8-15.
[53] W. Puff, X. Zhou, B. Oberdorfer, B. Scherwitzl, P. Parz, W. Sprengel, R. Wurschum, Comprehensive defect characterization of different iron samples after severe plastic deformation, J. Phys.: Conf. Ser. 443 (2013) 012033.

[54] K. Edalati, D. Akama, A. Nishio, S. Lee, Y. Yonenaga, J.M. Cubero-Sesin, Z. Horita, Influence of dislocation-solute atom interactions and stacking fault energy on grain size of single-phase alloys after severe plastic deformation using high-pressure torsion, Acta Mater. 69 (2014) 68-77.
[55] Y.J. Zhao, R. Massion, T. Grosdidier, L.S. Toth, Contribution of shear deformation to grain refinement and densification of iron powder consolidated by high pressure torsion, IOP Conf. Ser.: Mater. Sci. 63 (2014) 012032.
[56] A. Hosokawa, S. Ii, K. Tsuchiya, Work hardening and microstructural development during high-pressure torsion in pure iron, Mater. Trans. 55 (2014) 1097-1103.
[57] A. Hosokawa, H. Ohtsuka, T. Li, S. Ii, K. Tsuchiya, Micostructure and magnetic properties in nanostructured Fe and Fe-based intermetallics produced by high-pressure torsion, Mater. Trans. 55 (2014) 1286-1291.
[58] Y. Zhao, R. Massion, T. Grosdidier, L.S. Toth, Gradient structure in high pressure torsion compacted iron powder, Adv. Eng. Mater. 17 (2015) 1748-1753.
[59] H. Kato, Y. Todaka, M. Umemoto, M. Haga, E. Sentoku, Sliding wear behavior of sub-microcrystalline pure iron produced by high-pressure torsion straining, Wear 336-337 (2015) 58-68.
[60] C. Borchers, C. Garve, M. Tiegel, M. Deutges, A. Herz, K. Edalati, R. Pippan, Z. Horita, R. Kirchheim, Nanocrystalline steel obtained by mechanical alloying of iron and graphite subsequently compacted by high-pressure torsion, Acta Mater. 97 (2015) 207-205.
[61] A.M. Glezer, A.A. Tomchuk, T.V. Rassadina, Effect of the fraction and direction of high-pressure torsion deformation in a Bridgman cell on the structure and mechanical properties of commercial-purity iron, Russ. Metall. 2015 (2015) 295-300.
[62] S. Khoddam, P.D. Hodgson, A. Zarei-Hanzaki, L.Y. Foon, A simple model for material's strengthening under high pressure torsion, Mater. Des. 99 (2016) 335-340.
[63] L. Voronova, M. Degtyarev, T. Chashchukhina, D. Shinyavskii, T. Gapontseva, Effect of microcrystallites formed by deformation on the growth and orientation of grains during recrystallization of iron, Lett. Mater. 7 (2017) 359-362.
[64] R. Kulagin, Y. Zhao, Y. Beygelzimer, L.S. Toth, M. Shtern, Modeling strain and density distributions during high-pressure torsion of pre-compacted powder materials, Mater. Res. Lett. 5 (2017) 179-186.
[65] H. Iwaoka, M. Arita, Z. Horita, Hydrogen diffusion in ultrafine-grained iron with the body-centered cubic crystal structure, Philos. Mag. Lett. 97 (2017) 158-168.
[66] T. Leitner, A. Hohenwarter, W. Ochensberger, R. Pippan, Fatigue crack growth anisotropy in ultrafine-grained iron, Acta Mater. 126 (2017) 154-165.
[67] J. Todt, J. Keckes, G. Winter, P. Staron, A. Hohenwarter, Gradient residual strain and stress distributions in a high pressure torsion deformed iron disk revealed by high energy X-ray diffraction, Scripta Mater. 146 (2018) 178-181.
[68] P.W. Bridgman, Effects of high shearing stress combined with high hydrostatic pressure, Phys. Rev. 48 (1935) 825-847.
[69] P.W. Bridgman, High pressure polymorphism of iron, J. Appl. Phys. 27 (1956) 659.
[70] K. Edalati, Z. Horita, A review on high-pressure torsion (HPT) from 1935 to 1988, Mater. Sci. Eng. A 652 (2016) 325-352.
[71] T.J. Rupert, J.C. Trenkle, C.A. Schuh, Enhanced solid solution effects on the strength of nanocrystalline alloys, Acta Mater. 59 (2011) 1619-1631.

[72] J. Hu, Y.N. Shi, X. Sauvage, G. Sha, K. Lu, Grain boundary stability governs hardening and softening in extremely fine nanograined metals, Science 355 (2017) 1292-1296.
[73] E.O. Hall, The deformation and ageing of mild steel: III discussion of results, Proc. Phys. Soc. London B 64 (1951) 747-753.
[74] N.J. Petch, The cleavage strength of polycrystals, J. Iron Steel Inst. 174 (1953) 25-28.
[75] A.H. Chokshi, A. Rosen, J. Karch, H. Gleiter, On the validity of the hall-petch relationship in nanocrystalline materials, Scripta Metall. 23 (1989) 1679-1683.
[76] M.A. Meyers, A. Mishra, D.J. Benson, Mechanical properties of nanocrystalline materials, Prog. Mater. Sci. 51 (2006) 427-556.
[77] K.A. Padmanabhan, G.P. Dinda, H. Hahn, H. Gleiter, Inverse Hall-Petch effect and grain boundary sliding controlled flow in nanocrystalline materials, Mater. Sci. Eng. A 452-453 (2007) 452-453.
[78] P. Scardi, M. Leoni, R. Delhez, Line broadening analysis using integral breadth methods: a critical review, J. Appl. Cryst. 37 (2004) 381-390.
[79] A. Revesz, T. Ungar, A. Borbely, J. Lendvai, Dislocations and grain size in ball-milled iron powder, Nanostruct. Mater. 7 (1996) 779-788.
[80] K. Edalati, Z. Horita, H. Fujiwara, K. Ameyama, Cold consolidation of ball-milled titanium powders using high-pressure torsion, Metall. Mater. Trans. A 41 (2010) 3308-3317.
[81] X.Z. Liao, A.R. Kilmametov, R.Z. Valiev, High-pressure torsion-induced grain growth in electrodeposited nanocrystalline Ni, Appl. Phys. Lett. 88 (2006) 021909.
[82] H. Wen, Y. Zhao, Y. Li, O. Ertorer, K.M. Nesterov, R.K. Islamgaliev, R.Z. Valiev, E.J. Lavernia, High-pressure torsion-induced grain growth and detwinning in cryomilled Cu powders, Philos. Mag. 90 (2010) 4541-4550.
[83] S. Ni, Y.B. Wang, X.Z. Liao, S.N. Alhajeri, H.Q. Li, Y.H. Zhao, E.J. Lavernia, S.P. Ringer, T.G. Langdon, Y.T. Zhu, Grain growth and dislocation density evolution in a nanocrystalline Ni-Fe alloy induced by high-pressure torsion, Scripta Mater. 64 (2011) 327-330.
[84] S. Lee, K. Edalati, Z. Horita, Microstructures and mechanical properties of pure V and Mo processed by high-pressure torsion, Mater. Trans. 51 (2010) 1072-1079.
[85] K. Edalati, K. Imamura, T. Kiss, Z. Horita, Equal-channel angular pressing and high-pressure torsion of pure copper: evolution of electrical conductivity and hardness with strain, Mater. Trans. 53 (2012) 123-127.
[86] R.B. Figueiredo, M. Kawasaki, T.G. Langdon, An evaluation of homogeneity and heterogeneity in metals processed by high-pressure torsion, Acta Phys. Pol. A 122 (2012) 425-429
[87] M. Kawasaki, H.J. Lee, B. Ahn, A.P. Zhilyaev, T.G. Langdon, Evolution of hardness in ultrafine-grained metals processed by high-pressure torsion, J. Mater. Res. Technol. 3 (2014) 311-318.
[88] M. Kawasaki, R.B. Figueiredo, Y. Huang, T.G. Langdon, Interpretation of hardness evolution in metals processed by high-pressure torsion, J. Mater. Sci. 49 (2014) 6586-6596.
[89] N.Q. Chinh, R.Z. Valiev, X. X. Sauvage, G. Varga, K. Havancsak, M. Kawasaki, B.B. Straumal, T.G. Langdon, Grain boundary phenomena in an ultrafine- grained Al-Zn alloy with improved mechanical behavior for micro- devices, Adv. Eng. Mater.16 (2014) 1000-1009.

[90] K. Edalati, R. Uehiro, K. Fujiwara, Y. Ikeda, H.W. Li, X. Sauvage, R.Z. Valiev, E. Akiba, I. Tanaka, Z. Horita, Ultra-severe plastic deformation: evolution of microstructure, phase transformation and hardness in immiscible magnesium-based systems, Mater. Sci. Eng. A 701 (2017) 158-166.

[91] K. Edalati, Z. Horita, Significance of homologous temperature in softening behavior and grain size of pure metals processed by high-pressure torsion, Mater. Sci. Eng. A 528 (2011) 7514-7523.

[92] B. Srinivasarao, A.P. Zhilyaev, T.G. Langdon, M.T. Perez-Prado, On the relation between the microstructure and the mechanical behavior of pure Zn processed by high pressure torsion, Mater. Sci. Eng. A 562 (2013) 196-202.

[93] Y. Ito, K. Edalati, Z. Horita, High-pressure torsion of aluminum with ultrahigh purity (99.9999%) and occurrence of inverse Hall-Petch relationship, Mater. Sci. Eng. A 679 (2017) 428-434.

[94] K. Edalati, J.M. Cubero-Sesin, A. Alhamidi, I.F. Mohamed, Z. Horita, Influence of severe plastic deformation at cryogenic temperature on grain refinement and softening of pure metals: investigation using high-pressure torsion, Mater. Sci. Eng. A 613 (2014) 103-110.

[95] W.J. Botta Filho, J.B. Fogagnolo, C.A.D. Rodrigues, C.S. Kiminami, C. Bolfarini, A.R. Yavari, Consolidation of partially amorphous aluminium-alloy powders by severe plastic deformation, Mater. Sci. Eng. A 375-377 (2004) 936–941.

[96] A.P. Zhilyaev, S. Swaminathan, A.A. Gimazov, T.R. McNelley, T.G. Langdon: Using high-pressure torsion for the cold-consolidation of copper chips produced by machining, J. Mater. Sci. 43 (2008) 7451-7456.

[97] K. Edalati, Y. Yokoyama, Z. Horita, High-pressure torsion of machining chips and bulk discs of amorphous $Zr_{50}Cu_{30}Al_{10}Ni_{10}$, Mater. Trans. 51 (2010) 23-26.

[98] E.Y. Yoon, D.J. Lee, T.S. Kim, H.J. Chae, P. Jenei, J. Gubicza, T. Ungar, M. Janecek, J. Vratna, S. Lee, H.S. Kim, Microstructures and mechanical properties of Mg-Zn-Y alloy consolidated from gas-atomized powders using high-pressure torsion, J. Mater. Sci. 47 (2012) 7117-7123.

[99] K. Kramer, Y. Champion, R. Pippan, From powders to bulk metallic glass composites, Sci. Rep. 7 (2017) 6651.

[100] I. Fujita, K. Edalati, X. Sauvage, Z. Horita, Grain growth in nanograined aluminum oxide by high-pressure torsion: Phase transformation and plastic strain effects, Scripta Mater. 152 (2018) 11-14.

[101] K. Edalati, Q. Wang, H. Razavi-Khosroshahi, H. Emami, M. Fuji, Z. Horita, Low-temperature anatase-to-rutile phase transformation and unusual grain coarsening in titanium oxide nanopowders by high-pressure torsion straining, Scripta Mater. (2018) submitted.

[102] L. Balogh, T. Ungar, Y. Zhao, Y.T. Zhu, Z. Horita, C. Xu, T.G. Langdon, Influence of stacking-fault energy on microstructural characteristics of ultrafine-grain copper and copper-zinc alloys, Mater. Sci. Eng. A 56 (2008) 809-820.

[103] H.W. Zhang, X. Huang, R. Pippan, N. Hansen, Thermal behavior of Ni (99.967% and 99.5% purity) deformed to an ultra-high strain by high pressure torsion, Acta Mater. 58 (2010) 1698-1707.

[104] D.J. Lee, E.Y. Yoon, D.H. Ahn, B.H. Park, H.W. Park, L.J. Park, Y. Estrin, H.S. Kim, Dislocation density-based finite element analysis of large strain deformation behavior of copper under high-pressure torsion, Acta Mater. 76 (2014) 281-293.

[105] T. Ungar, S. Ott, P.G. Sandres, A. Borbely, J.R. Weertman, Dislocations, grain size and planar faults in nanostructured copper determined by high resolution X-ray diffraction and a new procedure of peak profile analysis, Acta Mater. 46 (1998) 3693-3699.
[106] N. Kamikawa, X. Huang, N. Tsuji, N. Hansen, Strengthening mechanisms in nanostructured high-purity aluminium deformed to high strain and annealed, Acta Mater. 57 (2009) 4198-4208.
[107] X. Huang, N. Kamikawa, N. Hansen, Strengthening mechanisms and optimization of structure and properties in a nanostructured IF steel, J. Mater. Sci. 45 (2010) 4761-4769.
[108] K. Edalati, Z. Horita, T. Furuta, S. Kuramoto, Dynamic recrystallization and recovery during high-pressure torsion: experimental evidence by torque measurement using ring specimens, Mater. Sci. Eng. A 559 (2013) 506-509.
[109] R.W. Armstrong, 60 Years of Hall-Petch: past to present nano-scale connections, Mater. Trans. 55 (2014) 2-12.
[110] S. Takaki, K. Kawasaki, Y. Kimura, Mechanical properties of ultra fine grained steels, J. Mater. Process. Technol. 117 (2001) 359-363.
[111] K. Takeda, N. Nakada, T. Tsuchiyama, S. Takaki, Effect of interstitial elements on Hall-Petch coefficient of ferritic, iron, ISIJ Int. 48 (2008) 1122-1125.
[112] S. Takaki, Review on the Hall-Petch relation in ferritic steel, Mater. Sci. Forum 654-656 (2010) 11-16.
[113] W.F. William, J. Hashemi, Foundations of Materials Science and Engineering, McGraw-Hill, New York, 2006.
[114] D. Tabor, The hardness of solids, Rev. Phys. Tech. 1 (1970) 145-179.
[115] J.A. Benito, R. Tejedor, R. Rodriguez-Baracaldo, J.M. Cabrera, J.M. Prado, Study of the plastic deformation in nanocrystalline and ultrafine iron and carbon steels, Mater. Sci. Forum 584-586 (2008) 617-622.
[116] T. Ungar, Characterization of nanocrystalline materials by X-ray line profile analysis, J. Mater. Sci. 42 (2007) 1584-1593.
[117] C.E. Carlton, P.J. Ferreira, What is behind the inverse Hall-Petch effect in nanocrystalline materials?, Acta Mater. 55 (2007) 3749-3756.
[118] J.B. Jeon, B.J. Lee, Y. Won Chang, Molecular dynamics simulation study of the effect of grain size on the deformation behavior of nanocrystalline body-centered cubic iron, Scripta Mater. 64 (2011) 494-497.
[119] T.D. Shen, R.B. Schwarz, S. Feng, J.G. Swadener, J.Y. Huang, M. Tang, J. Zhang, S.C. Vogel, Y. Zhao, Effect of solute segregation on the strength of nanocrystalline alloys: Inverse Hall-Petch relation, Acta Mater. 55 (2007) 5007-5013.
[120] G.E. Dieter, Mechanical metallurgy, McGraw-Hill, New York, 1961.

Table 1. Purity levels of Fe samples and their main impurities, initial states and grain sizes.

Purity	C (wt.%)	O (wt.%)	Cr (wt.%)	Ni (wt.%)	S (wt.%)	Initial State	Initial Grain Size
99.96%	0.0011	0.0014	<0.003		0.0014	Disc	140 μm
99.94%	0.0015		0.03	0.02	0.0041	Disc	33 μm
99.88%	0.002	0.11			0.007	Powder	10 μm
97.78%	0.07	0.75	0.89	0.49	0.016	Ball-milled	26 nm

Table 2. HPT processing conditions selected for examination of Fe samples with different purity levels.

Purity	Temperature (K)	Pressure (GPa)	Rotation Speed (rpm)	Number of Turns, *N*		
				Hardness Test	Tensile Test	TEM
99.96%	300	2	0.2	1/8, 1/4, 1/2, 1, 2, 4 , 10, 20	1/4, 1, 10	20
99.94%	300	6	1.0	1/4, 1/2, 3/4, 1, 2, 4, 10, 20	1/2, 1, 2, 10, 20	20
99.88%	300, 473	6	1.0	4, 10, 20	4, 10, 20	20
97.78%	473	6	1.0	4, 10, 20	4, 10, 20	20

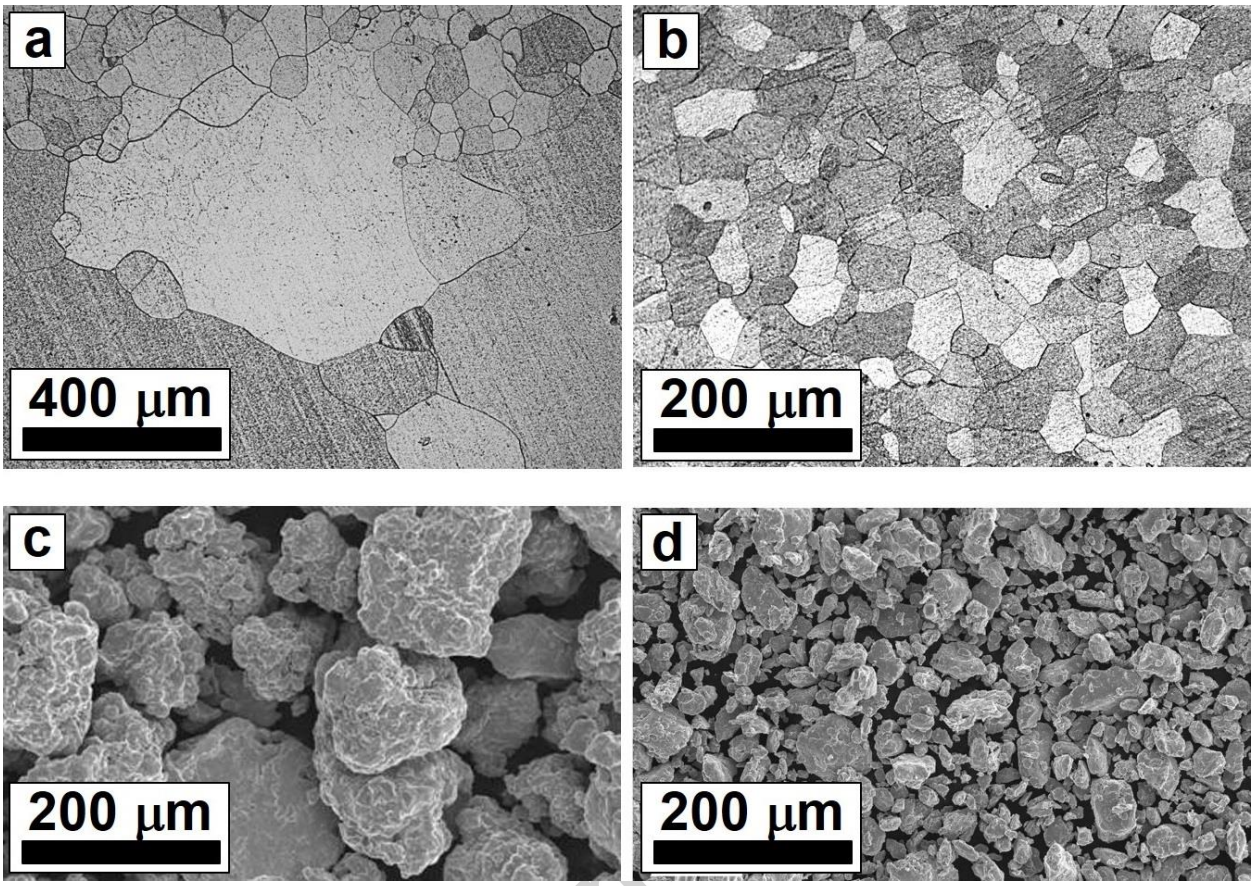

Figure 1. (a, b) Optical micrographs and (b, c) SEM micrographs for initial Fe samples with various purity levels as (a) 99.96%, (b) 99.94%, (c) 99.88% and (d) 97.78%.

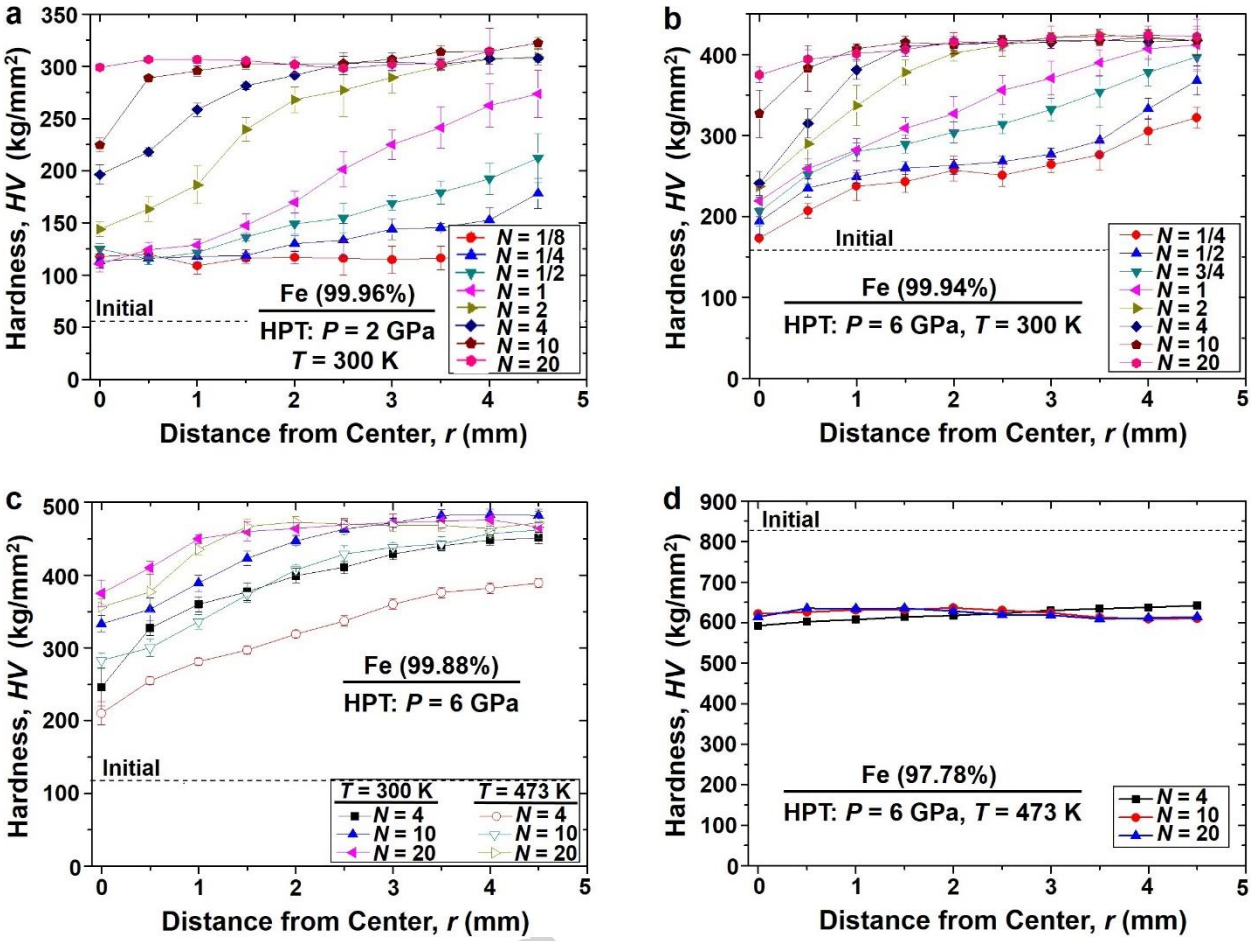

Figure 2. Variations of Vickers microhardness against distance from disc center for Fe with various purity levels as (a) 99.96%, (b) 99.94%, (c) 99.88% and (d) 97.78% after HPT processing under different conditions.

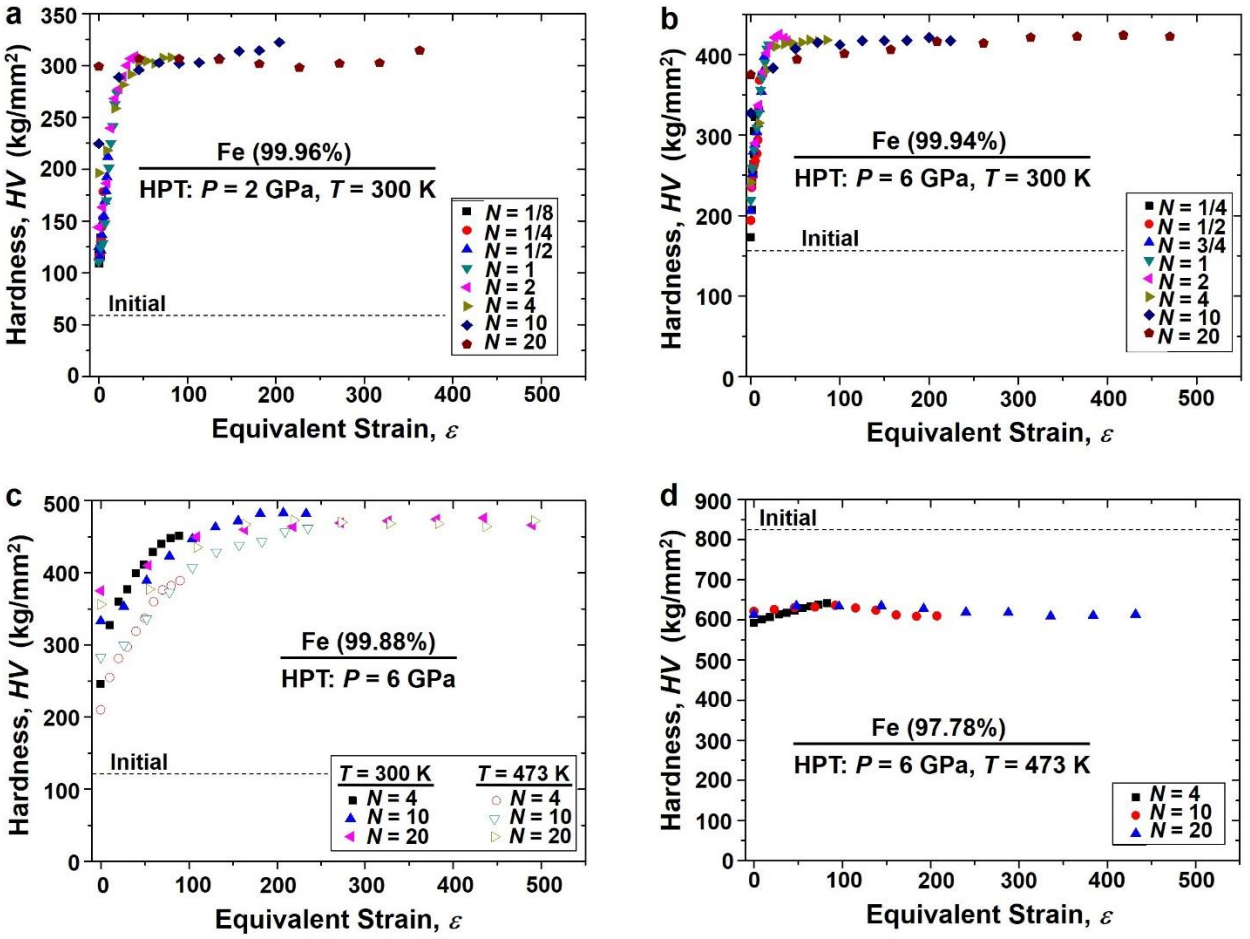

Figure 3. Variations of Vickers microhardness against von Mises equivalent strain for Fe with various purity levels as (a) 99.96%, (b) 99.94%, (c) 99.88% and (d) 97.78% after HPT processing under different conditions.

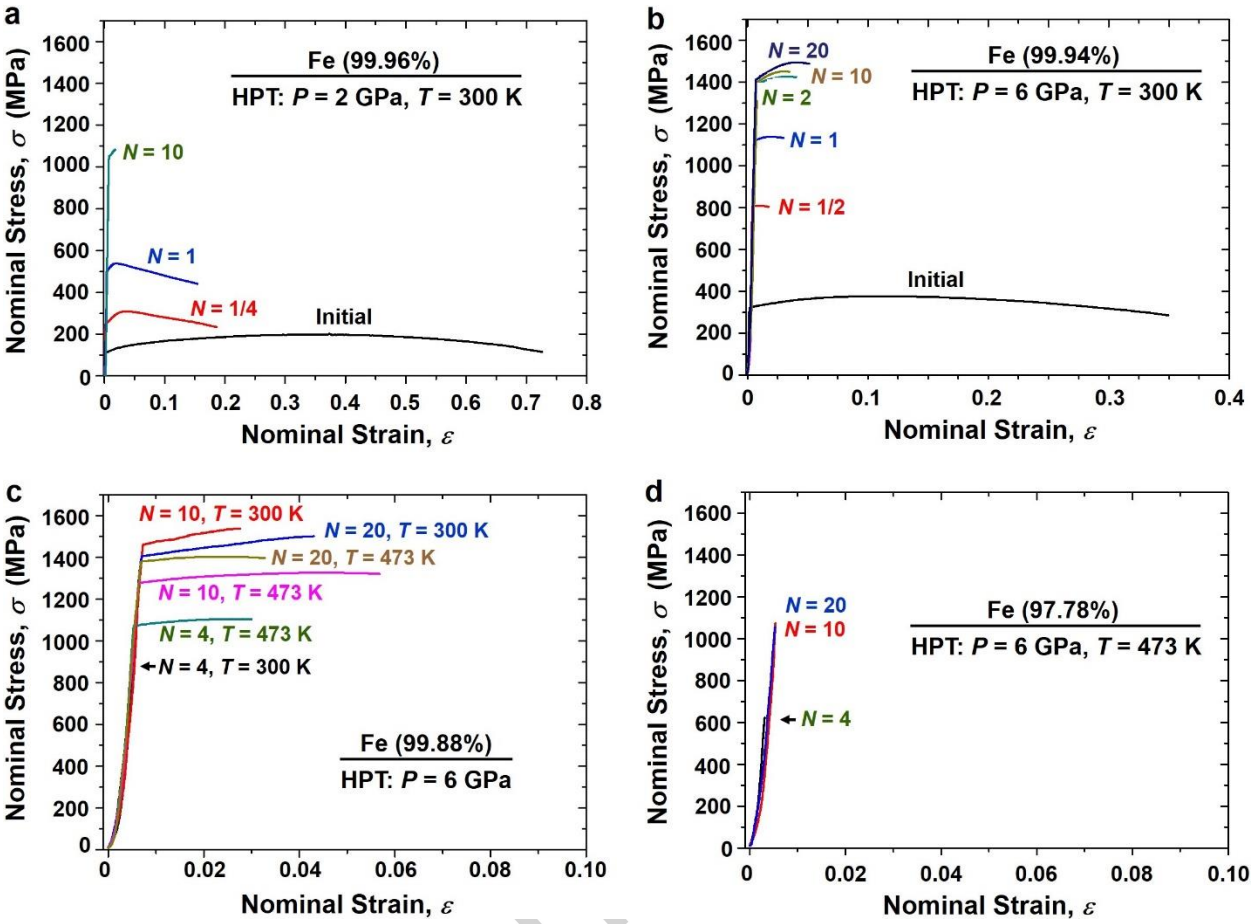

Figure 4. Tensile stress-strain curves for Fe with various purity levels as (a) 99.96%, (b) 99.94%, (c) 99.88% and (d) 97.78% after HPT processing under different conditions.

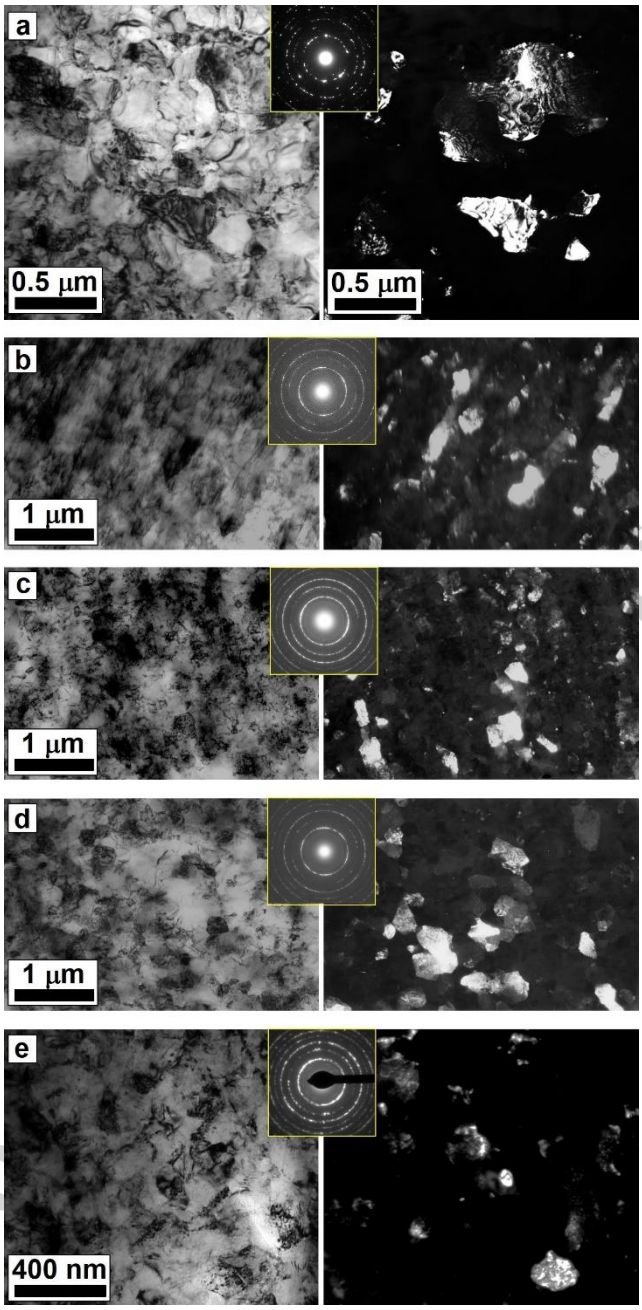

Figure 5. TEM bright-field images (left), dark-field images (right) and SAED patterns (center) for Fe with various purity levels as (a) 99.96%, (b) 99.94%, (c, d) 99.88% and (e) 97.78% after HPT processing for 20 turns at (a-c) 300 K and (d, e) 473 K.

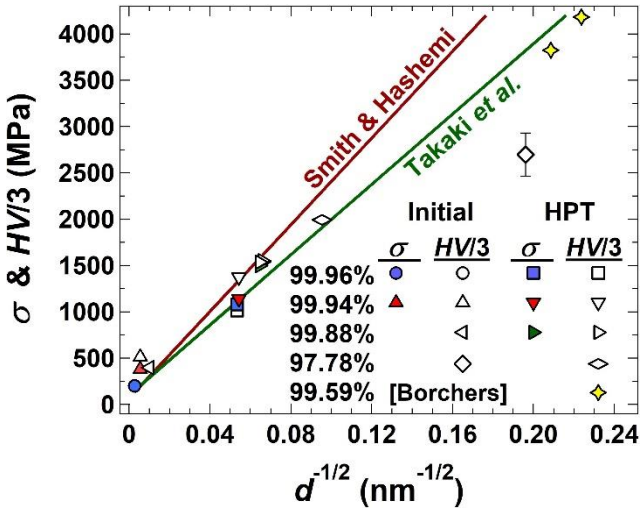

Figure 6. Variations of tensile strength (σ) and Vickers microhardness divided by 3 ($HV/3$) against inverse root of grain size ($d^{-1/2}$) for initial and HPT-processed Fe samples with various purity levels in comparison with Hall-Petch relationships reported by Takaki *et al.* for pure Fe [110-112] and by Smith and Hashemi for mild steels [113]. The data for sample with 99.59% purity was taken from Borchers *et al.* [60].

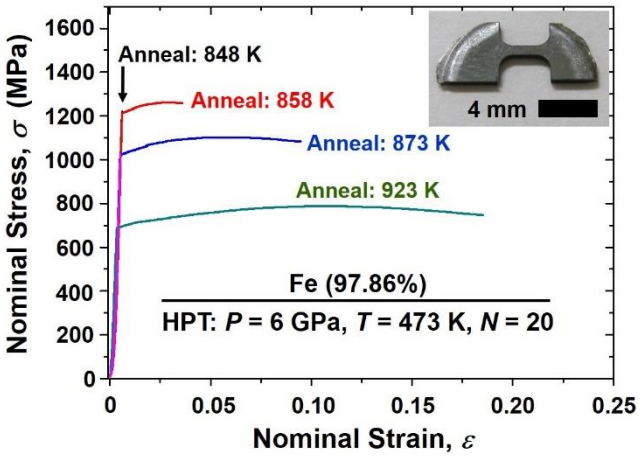

Figure A1. Tensile stress-strain curves for ball-milled Fe (97.78%) after HPT processing at 473 K for 20 turns and post-HPT annealing at different temperatures for 1 h. Inset appearance of tensile specimen before testing.

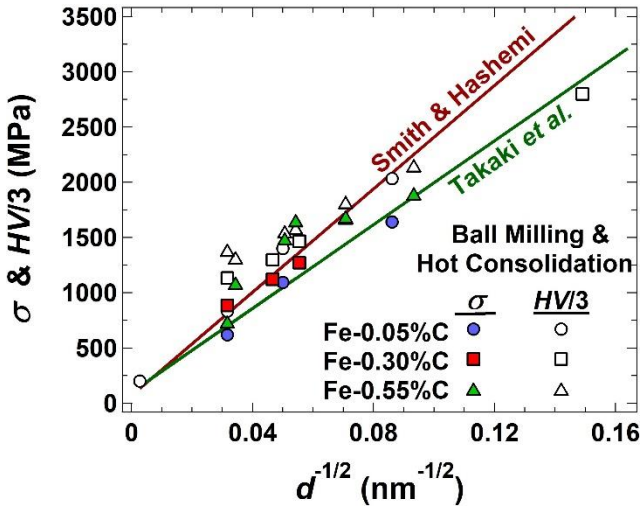

Figure A2. Variations of tensile strength (σ) and Vickers microhardness divided by 3 ($HV/3$) against inverse root of grain size ($d^{-1/2}$) for Fe samples with different carbon contents after ball milling followed by hot consolidation at different temperatures in comparison with Hall-Petch relationships reported by Takaki *et al.* for pure Fe [110-112] and by Smith and Hashemi for mild steels [113]. The data were taken from Benito *et al.* [115].